Journal of the Brazilian Society of Mechanical Sciences and Engineering (2026) 48:701
https://doi.org/10.1007/s40430-026-06646-6

TECHNICAL PAPER

Effects of infill pattern, infill ratio and print orientation on the mechanical and vibration response of PLA structures

Gökhan Haydarlar[1] · Mehmet Alper Sofuoğlu[2] · Tevfik Oğuzhan Ergüder[1] · Semih Duran[1]

Received: 13 January 2026 / Accepted: 30 May 2026
© The Author(s) 2026

Abstract

This study examined the combined effects of infill pattern, infill ratio, and pattern orientation on the tensile and vibration behavior of PLA structures produced by fused filament fabrication (FFF). Despite extensive studies on individual FFF parameters, the combined tensile and vibration behavior of honeycomb, tetrahedral, and Hilbert curve infills has not yet been systematically evaluated under a common structural parameter set. To address this gap, PLA specimens were manufactured using a Taguchi L9 design and evaluated by tensile testing and impact-based modal analysis. Pattern orientation governed the tensile response, accounting for about 60% of the variation in elastic modulus, 75% in tensile strength, and 67% in elongation. The highest elastic modulus was obtained in H45 (945.1 MPa), while T45 showed the highest tensile strength (40.3 MPa) and elongation (5.5%). In contrast, infill pattern was the main factor governing vibration behavior, accounting for about 59% of the stiffness variation and 80% of the damping ratio variation. Specifically, the Hilbert curve pattern showed the highest stiffness, while the tetrahedral pattern showed the highest damping ratio. Natural frequency was governed primarily by pattern orientation, which accounted for about 45% of the variation, while infill pattern had a secondary effect, contributing about 35%. HC45 exhibited the highest stiffness (450,000 N/m), T15 the highest damping ratio (0.128%), and T45 the highest natural frequency (195 Hz). These findings showed that mechanical strength and vibration response were controlled by different properties of internal architecture, providing a practical route for tailoring lightweight FFF components for engineering applications.

Keywords Additive manufacturing · FFF · PLA · Mechanical properties · Modal analysis

1 Introduction

Additive Manufacturing (AM) enables the fabrication of components with complex geometries and tailored internal architectures, providing significant design flexibility for engineering applications [1–4]. This capability has increased the need to optimize structural configurations not only in terms of mechanical performance but also with respect to vibration behavior, particularly in applications where lightweight and dynamic stability are critical. Although AM offers advantages such as reduced material waste and simplified production processes [5, 6], the effective utilization of its design flexibility for multifunctional performance remains a key challenge. Consequently, AM technologies have been widely adopted across various fields, including aerospace, automotive, medicine, bioengineering, and food technology, where both structural efficiency and vibration response are of importance [7–14].

AM production methods are categorized according to the type of energy source used or the primary feedstock material [15–17]. Among these, one of the most common and cost-effective AM methods is Fused Deposition Modeling (FDM), also known as Fused Filament Fabrication (FFF) or Material Extrusion (MEX) [18, 19]. FFF enables the low-cost fabrication of complex 3D components, test prototypes, lightweight tooling, and load-bearing parts [20, 21]. The production process operates by heating a filament feedstock until it reaches a semi-molten state and subsequently

Technical Editor: Zilda de Castro Silveira.

✉ Semih Duran
semih.duran@kafkas.edu.tr

[1] Faculty of Engineering and Architecture, Department of Mechanical Engineering, Kafkas University, Kars, Turkey

[2] Faculty of Engineering and Architecture, Department of Mechanical Engineering, Eskişehir Osmangazi University, Eskişehir, Turkey

Published online: 02 September 2026

Table 1 Previous studies

Study (full citation)	Material	Investigated parameters (levels)	Experimental design	n/replicates	Measured responses	Statistics/optimization	Main quantitative findings	Reported limitations
Buss et al. [45]	PLA	Infill density: 10, 30, 50, 70, 90%Print pattern: cubic, triangular Built-up direction: X, Y, Z	Multifactor experimental matrix (density—pattern—direction)	Total 150 specimens, at least 5 per configuration	ISO 178 three-point bending; flexural strength, together with printing time	Statistical method unspecified; comparative data evaluation reported	Best strength-time balance: Y direction + cubic + 90% infill, about 31 MPa with relatively low printing time	Limited to two pattern types; environmental conditions reported only as ambient laboratory conditions; detailed humidity/temperature protocol unspecified
Öteyaka et al. [1]	PLA	Infill pattern: Grid, Cross, Tri-hexagon. Infill ratio: 0, 20, 40, 60, 80, 100%	Parametric multi-level experimental study	At least 3 specimens per condition	Flexural strength and flexural modulus; damping/resonance behavior from impact-hammer-based modal analysis	Statistical method unspecified; comparative experimental analysis	Tri-hexagon showed the highest flexural strength; Cross showed higher damping capacity; flexural modulus and strength increased with infill ratio; the best damping was reported around 40% infill for all patterns	Environmental conditions and device calibration details are unspecified; scarcity of damping-focused studies emphasized
Singh et al. [46]	PLA	Filling percentage: 3 levels, exact values unspecified. Raster style: 3 levels, including concentric. Build orientation: horizontal, on-edge, vertical	Full factorial design, 3 factors and 3 levels	Total 27 tensile specimens	Ultimate tensile strength	ANOVA, with interaction observations also reported	Maximum UTS: on-edge + concentric raster, about 32.3 MPa; UTS increased with filling percentage; build orientation was one of the main determinants	Exact level values and environmental details unspecified; full interaction scope unspecified, although build orientation—raster style interaction was highlighted
Hikmat et al. [47]	PLA	Build orientation; raster orientation; nozzle diameter; extruder temperature; infill density; shell number; extrusion speed, level details partly unspecified	Taguchi mixed-model fractional design	18 experimental conditions; number of replicates unspecified	Tensile strength	S/N ratio, ANOVA, linear regression	According to ANOVA, the most influential factor was build orientation, about 44.7% contribution; nozzle diameter of 0.5 and infill density of 100% were also significant	Because many factors were included, higher-order interactions may not have been fully resolved; environmental conditions and calibration details are unspecified
Bonada et al. [48]	PLA	Infill pattern: Grid, Linear090 (0/90), Linear45 (45) Printing orientation: Flat, On-edge, Vertical	Multi-group experimental study plus FEM RVE/homogenization approach	3 patterns × 3 orientations × 5 specimens = 45 tensile tests	Elastic modulus, Poisson's ratios, stress–strain behavior	Experimental tests plus FEM-based estimation of effective elastic constants	Linear 090 gave a higher elastic modulus; Grid had the lowest mechanical properties and was not recommended for parts requiring high stiffness	FEM-RVE limitations clearly discussed, including linear-range assumption and modelling only the internal pattern; surface skin effects also noted

Table 1 (continued)

Study (full citation)	Material	Investigated parameters (levels)	Experimental design	n/replicates	Measured responses	Statistics/optimization	Main quantitative findings	Reported limitations
Medel et al. [39]	PLA	Build orientation: on-flat, on-edge. Raster angle: 0, 45, 90. Nozzle temperature: 200, 220°CPrint speed: 60, 120 mm/s Layer height: 0.1, 0.25 mm	DOE with 48 combinations	48 combinations × 2 specimens = 96	Modal frequencies and amplitudes by LDV; equivalent elastic modulus; damping ratio; transmissibility area	Statistical tests, including normality, t-test/Wilcoxon; CLT-based stiffness and damping models	Low temperature, 200 °C, and high speed, 120 mm/s, were associated with low stiffness and high damping, interpreted as weak inter-filament bonding; high damping may indicate poor filament bonding	Infill pattern and density were not varied; environmental details unspecified
He et al. [43]	ABS, cantilever beams	Nozzle size: 0.4, 0.6, 0.8 mm. Infill density: 40, 60, 80, 100%. Infill pattern: line, gyroid, cubic, triangles, with raster sub-levels for line	Multifactor DOE, 72 combinations	3 specimens per combination; total 72 combinations	First-mode damping ratio; loss factor; stiffness as an intermediate variable	ANOVA, correlation, regression, multivariate polynomial models	Damping ratio decreased as infill density increased; pattern type and nozzle size were also significant; damping ratio increased as nozzle size decreased	Categorical pattern variable was difficult to include in some regression models, so pattern was excluded from some formulations; study used ABS rather than PLA
Gonabadi et al. [49]	PLA	Raster angle: 0, 45, 90. Build orientation: on-edge 0, 45, 90 and flat. Infill density: 50% and 100%, rectilinear 0/90	Experimental study plus multi-scale FEM, RVE homogenization and explicit microstructure	Number of specimens/replicates unspecified; study included experimental validation against FEM	Elastic constants and elastic response in bending, tension, and shear; FEM-based stress concentration and interface behavior	FEM homogenization, explicit microstructure modelling, experimental validation	Increasing build/raster angle from 0 to 90 caused an experimental flexural modulus drop of about 31 to 32%; FEM predicted the same trend; infill density was emphasized as the most influential factor	Modelling limited to the elastic regime; viscoelastic and plastic behavior not included; need for improved modeling at partial infill, such as 50% discussed

extruding the material through a heated nozzle in a layer-by-layer manner [22–24]. In the FFF methods, a wide range of thermoplastic materials such as Polylactic Acid (PLA), Acrylonitrile Butadiene Styrene (ABS), Polycarbonate (PC), and Thermoplastic Polyurethane (TPU) as well as their composites (e.g., PLA/CF, ABS/CF) can be used as feedstock materials [25–32]. In particular, PLA was selected as it is a widely used FFF material suitable for evaluating mechanical and vibration behavior [1, 2, 15, 33, 34].

There are numerous process parameters that influence the quality and final properties of parts produced by FFF, and further research is required to determine optimal manufacturing settings. These parameters can be categorized into manufacturing parameters (nozzle temperature, print speed, etc.) and structural parameters (infill ratio, raster angle, nozzle size, layer thickness, infill pattern, etc.) [35–39]. The infill ratio is a key parameter that defines the material density inside the model and plays a critical role in optimizing both material usage and printing time. Previous studies have consistently shown that increasing the infill ratio leads to improvements in mechanical properties such as tensile and flexural strength, while lower infill ratios may provide advantages in terms of specific strength and material efficiency [1, 40]. Similarly, studies investigating different infill patterns have reported that structural configuration significantly influences load-carrying capacity and strength, with pattern geometry and raster alignment governing the mechanical response of FFF parts [35, 40]. Print orientation and raster angle refer to the orientation of the part to be produced on the build platform and have a decisive impact on the mechanical properties of FFF parts due to their anisotropic nature [41, 42]. In general, studies have shown that the alignment between the loading direction and the internal structure plays a critical role. Orientations aligned with the load improve strength, while perpendicular configurations tend to enhance energy dissipation and affect failure behavior [43, 44]. To provide a critical and structured overview of the literature, selected representative studies were comparatively summarized in Table 1 according to their investigated parameters, measured responses, and evaluation methods. This information presented indicates that previous studies have provided valuable findings on the effects of FFF parameters on polymer structures. However, most of them focused on either mechanical properties or vibration-related responses. Although some studies included statistical or numerical evaluations, these approaches were generally applied to a restricted set of responses rather than to a combined mechanical–dynamic assessment. Therefore, a unified evaluation of tensile behavior, modal response, and contribution-based statistical analysis under the same experimental design remains insufficiently addressed.

While neat PLA is generally unsuitable for primary load-bearing machinery components due to its limited mechanical strength and thermal stability, understanding its dynamic behavior is critical for several engineering applications. FFF-printed PLA is extensively used for lightweight auxiliary components, such as robotic end-effectors, UAV frames, sensor brackets, and custom manufacturing fixtures, where components must withstand operational vibrations without reaching destructive resonance. Furthermore, polymer structures exhibit highly advantageous viscoelastic damping properties compared to metals. Consequently, PLA serves as a highly accessible and effective surrogate material for experimentally validating how complex, bio-inspired, or mathematically derived internal architectures (such as varying infill patterns) can be utilized to intentionally tune the stiffness, natural frequency, and damping ratios of lightweight parts.

Materials' responses to vibration, alongside their mechanical strength properties, constitute a critical factor to control in machinery systems. Although stiffness, natural frequency, and damping behavior have been investigated in various material systems such as composite structures, sandwich panels, and numerical models [50–55], these studies do not directly address FFF-fabricated PLA structures. In addition, a combined evaluation of mechanical and vibration behavior under the same structural parameters remains limited for FFF-produced polymer components. Regarding damping capacity, among the patterns examined (Grid, Cross, and Tri-hexagon), the best vibration damping properties were typically observed at a 40% infill ratio. Among these, the cross pattern exhibited the most effective vibration damping behavior, as it was thought to help dissipate vibrations by elongating the path for vibration signals [1]. Additionally, it was reported that raster angle significantly affected vibration damping, with raster orientations perpendicular to the loading axis providing higher damping [56]. Previous studies reported that print orientation plays a critical role in governing stiffness and natural frequency, where orientations perpendicular to the vibration axis tend to increase both parameters. Furthermore, processing parameters such as infill structure and manufacturing conditions were shown to significantly affect dynamic behavior, including natural frequency and damping characteristics [57, 58]. In this context, the combined and interactive effects of the infill pattern, infill ratio, and print orientation parameters on both mechanical and vibration behavior, as well as the statistical contribution of each parameter to these responses, have not been clearly established in previous studies.

In this study, the infill pattern, infill ratio, and print orientation parameters were selected considering their fundamental roles in governing internal load paths, material distribution, and anisotropic behavior in FFF structures. PLA specimens

Table 2 Printing parameters used during specimen fabrication

Printing parameters	Value
Layer thickness (mm)	0.20
Nozzle temperature (°C)	190
Build platform temperature (°C)	50
Wall count	2
Top and bottom layers count	4
Cooling fan speed (%)	100
Printing speed (mm/s)	100
Nozzle material	Brass
Nozzle diameter (mm)	0.40

were manufactured using a Taguchi L9 experimental design, and their performance was evaluated through a combined approach involving tensile testing and impact-based modal analysis. Unlike commonly used simple infill geometries (e.g., rectilinear or cubic patterns), honeycomb, tetrahedral, and Hilbert curve patterns were selected in this study due to their distinct structural characteristics and load transfer mechanisms. As a result of our literature review, no study was found that investigates the combined mechanical and vibration behavior using these infill patterns. The effects of the selected parameters were assessed using signal-to-noise (S/N) ratios and contribution analyses to identify their relative influence on different performance metrics. This study provided a unified evaluation of mechanical and dynamic responses under the same structural parameter set. It further demonstrated that infill design could be utilized as a controllable engineering variable to tailor both strength and vibration characteristics. In this context, it is anticipated that different infill designs can be used as performance-enhancing structural features in vibration-sensitive systems (such as sensor housings, robotic joints, and drone components), as well as in lightweight load-bearing parts, damper-like polymer elements, and functional prototypes.

2 Experimental

In this study, the effects of process parameters on the mechanical and vibrational properties of PLA specimens manufactured by the FFF method were examined. Tensile tests and modal analyses were applied to the produced specimens. The specimens were first designed in SolidWorks, and the resulting geometries were exported in STL format and imported into Creality Print 6.3. Then, using the predetermined printing parameters, the models were sliced to generate the G-codes and manufactured with a Creality Ender 3 V3 SE FFF-based 3D printer. To ensure consistency throughout the manufacturing process, the printing parameters were kept constant and were detailed in Table 2.

All prints were carried out at room temperature under identical manufacturing conditions. Ender PLA+white filament was used as the material for specimen production. Considering the number of process parameters and their potential interactions, the Taguchi L9 orthogonal array was selected to design the experiments in an efficient and systematic manner. This design allowed the main effects of infill pattern, infill ratio, and pattern orientation to be evaluated using only nine factor combinations. In addition, the Taguchi methodology provided S/N ratios and analysis of variance, enabling a robust identification of the most influential parameters under experimental scatter and guiding the selection of parameter combinations that enhance both mechanical and vibration performance. For each parameter combination in the design, three identical specimens were produced, resulting in a total of 27 specimens. The specimen's nomenclature and the Taguchi experimental design were presented in Table 3. The selected infill patterns (honeycomb, tetrahedral, and Hilbert curve) were chosen to represent distinct structural architectures with different load transfer characteristics, including planar, three-dimensional, and fractal-based geometries. This selection was made to enable the evaluation of the influence of advanced internal architectures on mechanical and vibration behavior.

Table 3 Taguchi L9 experimental design and nomenclature of specimens

Specimen	Infill pattern	Infill ratio (%)	Pattern orientation (°)
H15	Honeycomb	15	0
H30		30	45
H45		45	90
HC15	Hilbert curve	15	45
HC30		30	90
HC45		45	0
T15	Tetrahedral	15	90
T30		30	0
T45		45	45

The Taguchi L9 array used in this study was intended to identify the dominant main effects of three three-level factors with a limited number of experiments. For this reason, it does not independently capture the interaction terms of infill pattern—infill ratio, infill pattern—pattern orientation, infill ratio—pattern orientation, or the three-way interaction. Main effects were considered sufficient because the purpose of the Taguchi L9 design in this study was to screen and rank the dominant contributions of three three-level structural parameters with a manageable number of experiments, rather than to quantify all interaction terms. This was consistent with the manuscript's stated objective and with the ANOVA results, which showed clear dominance of single factors for most responses. The use of three specimens for each parameter combination provided a basic estimate of experimental scatter, improved the robustness of the average response values, and increased confidence that the

observed differences reflected systematic parameter effects rather than isolated specimen-level variability.

During the FFF manufacturing process of the specimens, the internal structure visuals corresponding to the infill pattern and infill ratio, as well as the schematic representation of pattern orientation variations, were presented in detail in Fig. 1. Pattern orientation was defined by the angle between the long edge of the specimen and the Z-axis on the build platform. The specimens were produced in a manner that ensured consistency in factors such as heat distribution and distance from the build platform center, which could affect print quality.

The specimens were produced according to the ASTM D638-14 standard using a Type IV specimen geometry to determine their mechanical behavior. The specimen thickness was selected as 3.2 mm. Images of the specimens after production were presented in Fig. 2.

Prior to testing, the specimens were kept under laboratory room-temperature conditions, and all tests were conducted under the same environmental conditions. No additional humidity-controlled conditioning protocol was applied. Although this procedure ensured comparable testing conditions for all specimens, the absence of a humidity-controlled conditioning protocol should be considered a limitation of the study, since moisture exposure may influence the

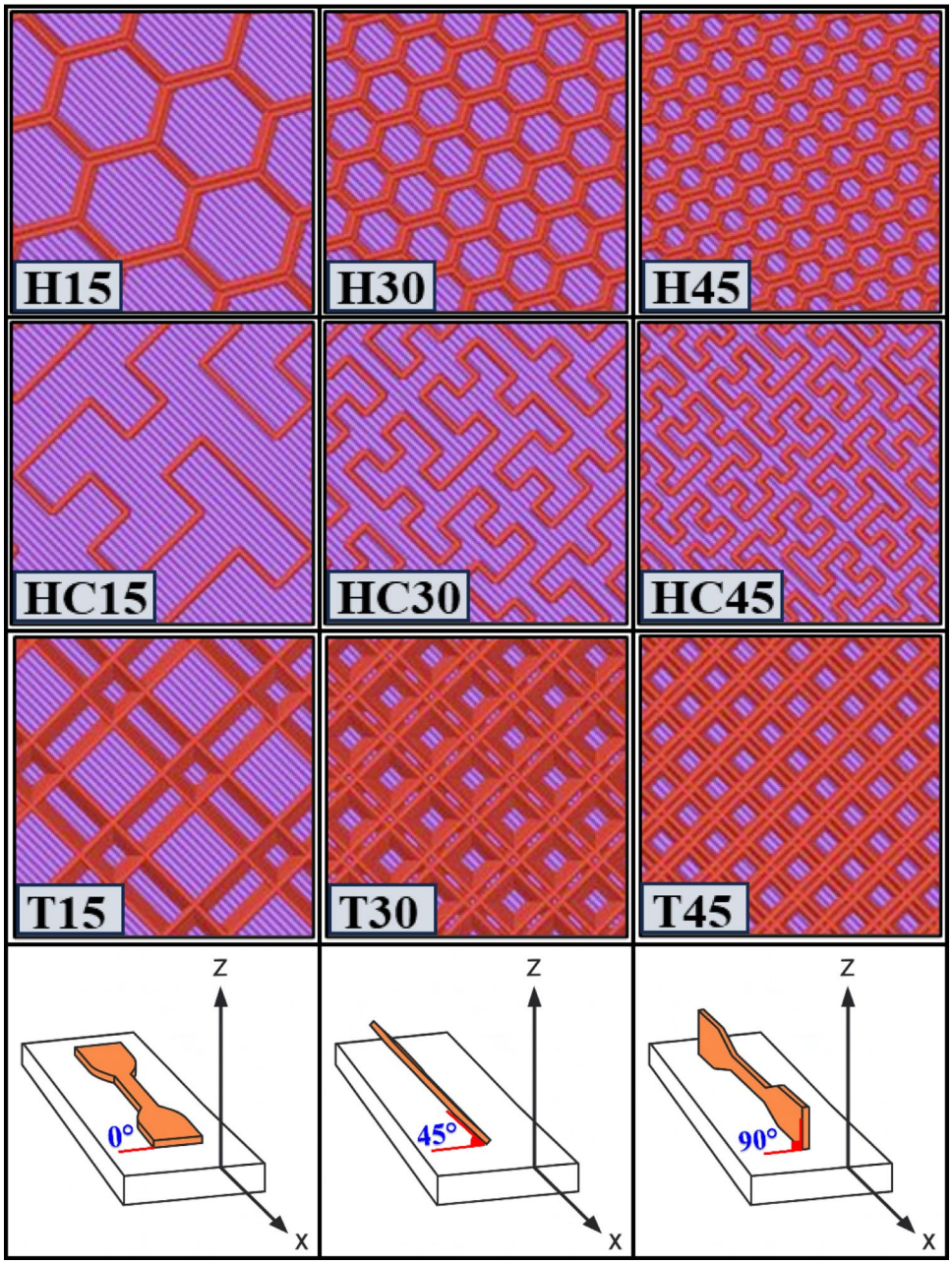


Fig. 1 Infill structure and variation of pattern orientation of the specimens

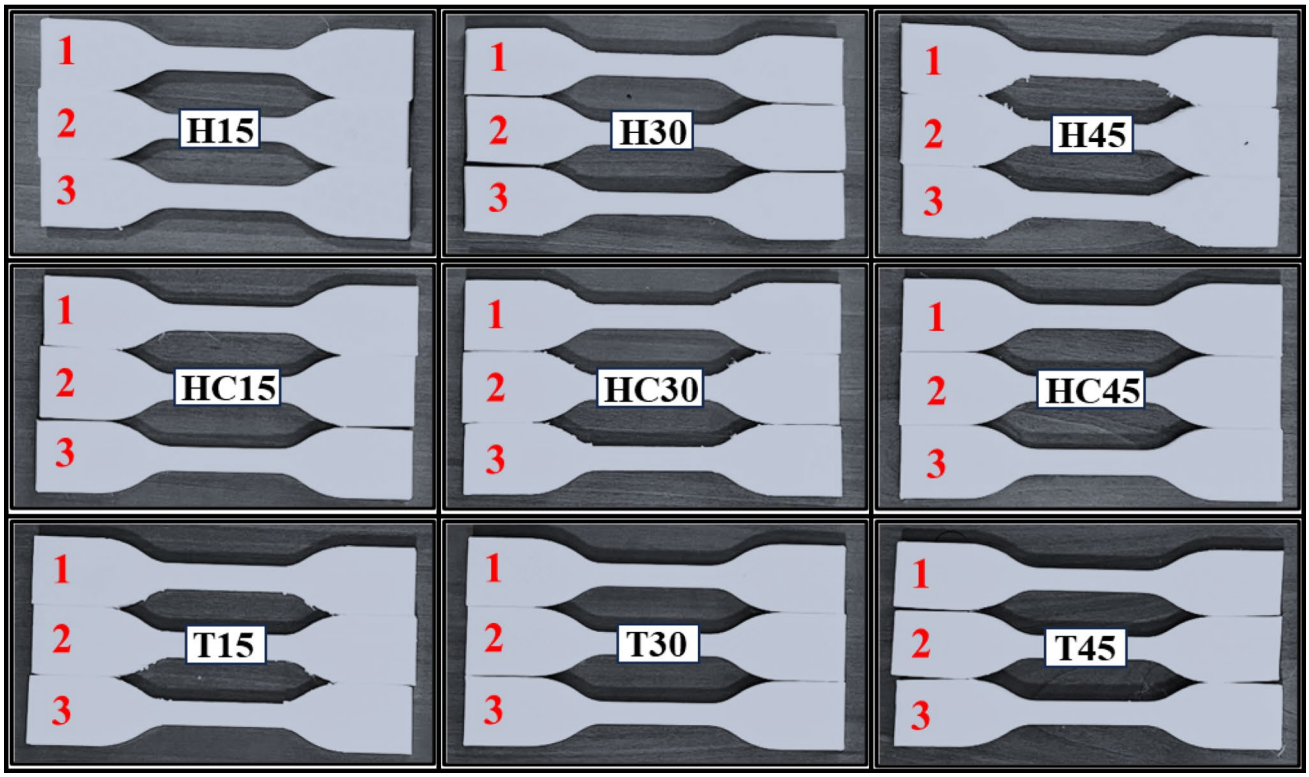


Fig. 2 Produced tensile specimens

mechanical and dynamic response of FFF-printed PLA structures.

Tensile testing, a fundamental step in mechanical characterization, was conducted to determine the behavior of the produced specimens under uniaxial loading. This test is critical for revealing the material's elastic and plastic deformation characteristics, elongation, and tensile strength. During the tensile test, the specimens were fixed at both ends and loaded so that they were pulled apart at a constant speed along their longitudinal axis. As the load increased, tensile stresses began to accumulate in the fracture region, causing the material to first reach its elastic limit, then the yield region, and finally the point of fracture. The tensile tests were performed using a universal testing machine operating under its routine calibrated configuration. The machine load cell was verified according to the manufacturer's calibration procedure before the testing, and all specimens were tested under identical loading conditions at a crosshead speed of 5 mm/min. Prior to testing, all specimens were inspected for dimensional accuracy and surface integrity. Tests were conducted at room temperature under consistent loading conditions to ensure repeatability of results. The elastic modulus, tensile strength, and elongation values were determined from the load–displacement curves using standard engineering stress–strain relations. Engineering stress and strain were calculated a $\sigma = F/A_0$ and $\varepsilon = \Delta\ell/\ell_0$, respectively. The tensile strength was obtained as $\sigma_{ts} = F_{\max}/A_0$. The elastic modulus ($E$) was calculated by converting the initial linear region of the load–displacement curve into the corresponding engineering stress–strain response. The strain at break was calculated as $\varepsilon_{break} = \Delta\ell_{break}/\ell_0$. Here,$F$ is the applied load,$F_{\max}$is the maximum load,A_0 is the initial cross-sectional area,$\Delta\ell$ is the change in gauge length,$\Delta\ell_{break}$ is the elongation at fracture, and ℓ_0 is the initial gauge length. In all calculations, the initial cross-sectional area of the specimens was taken as 19.2 mm^2.

Impact-based modal analysis was conducted to evaluate the dynamic behavior of the specimens. Modal analysis is a fundamental technique that determines a structure's natural frequencies, mode shapes, and damping characteristics, enabling a comprehensive assessment of structural performance under vibration. In this study, to replicate boundary conditions similar to those in the tensile test, each specimen was fixed at both ends using vices, as shown in Fig. 3, and controlled impacts were applied to the tensile region using an impact hammer. Vibration responses following the impacts were recorded via accelerometers attached to the tensile region and analyzed using Cut Pro 8.0 software. To reliably characterize the vibration properties of each specimen, five consecutive impacts were performed. The collected data were curve-fitted to calculate the specimens' natural frequencies, stiffness, and damping ratios. The

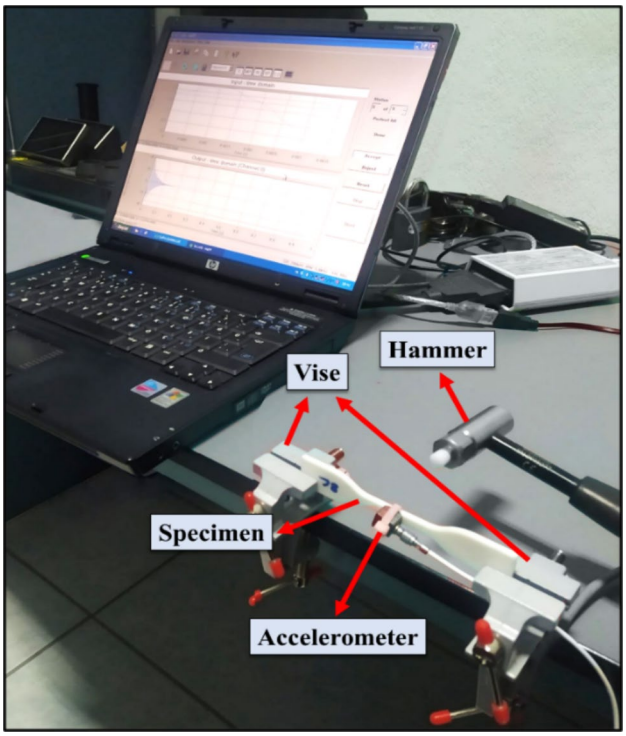


Fig. 3 Modal analysis measurements of specimens

tests were conducted under the same sensor configuration, impact location, and environmental conditions for all specimens. This ensured the comparability and repeatability of the dynamic behavior of PLA specimens produced with different parameters.

A PCB 7902 impact hammer, controlled by swing angle for constant force, was used for impact testing at the midspan, with three repetitions to minimize error. Damping ratios were calculated using the half-power bandwidth method. Potential errors from hammer velocity and mounting led to an estimated overall error margin of ± 5% in the damping ratio, sufficient for comparative defect analysis. The hammer and an accelerometer were connected to a data acquisition system via an interface unit. Post-data collection, curve fitting optimized modal characteristics, yielding natural frequencies and damping coefficients. Also, the Frequency Response Function (FRF) or the Transfer Function (TF) was measured using an impulse hammer test-based system by capturing and averaging successive impulse-mode TF readings from a specified number of specimens.

The experimental setup utilized a PCB 9690 accelerometer, characterized by a sensitivity of 5.17 mV/g (with conversion factors of $ms^2 = 0.102$ g and 1.28 g). For excitation, a PCB 7902 hammer/force sensor, equipped with a steel tip and featuring a sensitivity of 0.22 mV/N, was employed. To ensure measurement reliability and repeatability, each modal test was performed three times under consistent conditions. The consistency across these repeated tests, with any minor deviations falling within an acceptable range, confirmed the robustness of the data and the resulting conclusions from the modal analysis.

The accelerometer measurements were acquired using the MALTF/CutPro measurement chain with an instrumented impact hammer, accelerometer, and NI data acquisition hardware. Prior to testing, the measurement setup was configured by entering the manufacturer-provided sensitivity values of the hammer and accelerometer into the software, enabling ICP power for the active channels, and scaling the transfer function accordingly through the gain settings.

The natural frequency of a system depends on the mode of vibration and is a function of elastic deformation and mass. It was expressed by the Euler–Bernoulli equation presented in Eq. 1. In this equation, ω denotes the natural frequency, ρ is the material density, E is the elastic modulus, I is the area moment of inertia, A corresponds to the cross-sectional area, and l indicates the beam length. The parameter βl varies depending on the boundary conditions of the beam. For beams with fixed–fixed boundary conditions, the values of βl corresponding to the first three mode shapes are 4.73, 7.85, and 10.99, respectively [59].

$$\omega = (\beta l)^2 \sqrt{\frac{EI}{\rho A l^4}} \tag{1}$$

Although Eq. 1 applied to homogeneous, isotropic, prismatic beams with idealized kinematic assumptions, it was used here only as a simplifying reference to illustrate that variations in effective stiffness and mass distribution can alter the natural frequency. These assumptions are not fully satisfied in FFF-printed specimens because the infill architecture introduces anisotropy, non-uniform load-transfer paths, localized density variations, and possible interlayer compliance. Therefore, the Euler–Bernoulli formulation should be interpreted as a conceptual framework rather than a quantitative predictive model for the present structures. Although more advanced approaches, such as Timoshenko beam modeling or finite element analysis, provide a more accurate representation of the dynamic response of such non-homogeneous printed specimens, they were not included within the scope of the present experimental study. Accordingly, rather than claiming direct analytical verification, the present study relied on repeated FRF measurements and the consistency of the experimentally observed resonance trends as a practical alternative for assessing the physical validity of the modal response.

3 Results and discussions

3.1 Tensile testing for mechanical response

The load–displacement graphs for all specimens were presented in Fig. 4. The near-complete overlap of the three repetitions within each specimen group confirmed both the stability of the manufacturing process and the reliability of the experimental measurements. Examination of the graphs showed that a distinct linear region appeared in all specimens, followed by a short transition region that led to the maximum load after elastic deformation. With increasing infill density, a pronounced improvement in load-carrying capacity was observed, particularly in the honeycomb and tetrahedral patterns. In contrast, the Hilbert curve pattern exhibited the opposite trend, revealing the differing influences of geometric continuity on load transfer. The slope and load values reached by the T45 specimens in the elastic region showed that the internal structural characteristics of this pattern improved the mechanical response. Since the pattern type directly determined the continuity of the load transfer paths, the honeycomb and tetrahedral structures formed a more efficient load-bearing structure, providing higher strength compared to the Hilbert curve pattern [60, 61]. Mechanical performance was not directly related to the pattern orientation, but instead maximum tensile loads were obtained as a result of a more compatible match between the infill pattern and the tensile direction in specific combinations (H45, HC30, T45).

Figure 5 presented the tensile test results of the specimens along with their corresponding S/N ratios. The highest elastic modulus values were calculated as 945.1 ± 24.9 MPa,

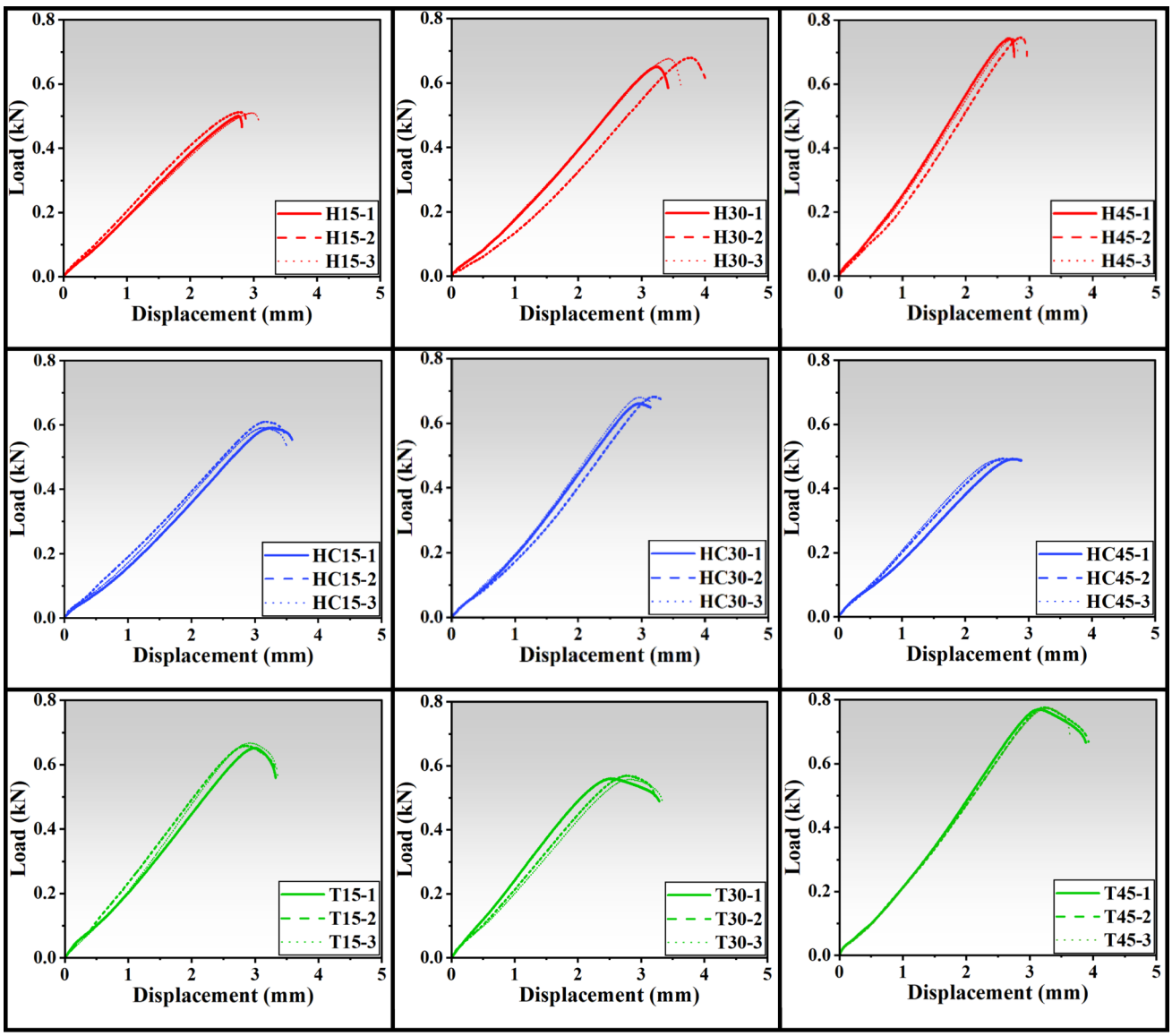


Fig. 4 Load–displacement graphs of specimens

758.1 ± 19.3 MPa, and 730.0 ± 30.0 MPa for the H45, HC30, and T45 specimens, respectively. It was evident that load transfer occurred more stably in these specimens, and the resistance to deformation in the elastic region increased. Similarly, previous studies emphasized the decisive effect of pattern orientation on mechanical performance [62–64]. This was attributed to the low elastic modulus values observed in the H15, HC45, and T30 specimens with a 0° pattern orientation, where the internal infill lines were aligned perpendicular to the loading direction and initial deformation developed more easily. This trend demonstrated that in FFF manufacturing, the pattern was not merely a geometric choice but a functional parameter controlling the elastic response. According to ANOVA results, the contributions of infill pattern, infill ratio, and pattern orientation to the elastic modulus were determined as 7.4%, 29.2%, and 60.0%, respectively. These results showed that the elastic modulus was sensitive to both the infill ratio and, especially, the pattern orientation. The fact that pattern orientation alone accounted for the majority of the total effect confirmed that pattern orientation was the most critical parameter in elastic behavior.

The highest tensile strength values calculated were 38.8 ± 0.6 MPa, 35.2 ± 1.0 MPa, and 40.3 ± 0.6 MPa for the H45, HC30, and T45 specimens, respectively. The more effective alignment of the infill pattern with the load-bearing direction delayed crack initiation, allowing the specimens to reach maximum stress values. The high strength observed particularly in the T45 specimen resulted from the cross-oriented infill lines distributing the load more homogeneously and increasing the energy accumulation capacity before fracture. In the specimens exhibiting the lowest strength (H15, HC45, and T30), the pattern orientation caused localized stress accumulation, which led to earlier failure. According to ANOVA results, the most dominant parameter controlling tensile strength was pattern orientation, with a contribution of 74.5%. With contribution levels of approximately 10–11%, the infill pattern and infill ratio exhibited considerably lower effects. Therefore, it was evident that the orientation of the pattern geometry with respect to the loading direction directly influenced the tensile strength [65].

The H30 (5.3 ± 0.3%), HC15 (5.1 ± 0.1%), and T45 (5.5 ± 0.2%) specimens exhibited the highest elongation values. These specimens possessed a 45° pattern orientation, where the internal infill lines contributed maximally to the slip planes under load. This orientation facilitated plastic deformation, delayed crack propagation, and significantly enhanced ductility by increasing the material's energy absorption capacity [66]. Additionally, the effective transfer of load to regions where the crystalline polymer chains of PLA were aligned contributed to the deformation ability of the material. Analysis of the ANOVA results revealed that pattern orientation was the most influential parameter for elongation, accounting for 66.8% of the total contribution. The infill pattern exhibited a meaningful yet secondary effect with its 19.2% contribution, indicating that the pattern geometry can influence the deformation behavior. Likewise, the filling ratio contributed 10.8%, indicating that changes in density had a slight effect on elongation. These findings revealed that elongation was chiefly controlled by the deformation of infill lines under load, while the infill pattern and infill ratio provided additional, non-negligible contributions to the specimens' deformation capability.

The ANOVA contribution analysis showed that pattern orientation was the dominant factor governing the mechanical responses, with contribution ratios of 60.0% for elastic modulus, 74.5% for tensile strength, and 66.8% for elongation. Among these, orientation was statistically significant for tensile strength ($p = 0.045$) and elongation ($p = 0.017$), while its effect on elastic modulus was close to the significance threshold ($p = 0.053$). These results indicated that the alignment of the internal structure with the loading direction plays a decisive role in the tensile behavior of FFF-printed PLA specimens. This dominant contribution of pattern orientation was consistent with the anisotropic nature of FFF-printed PLA structures reported in the literature [41, 62]. In this study, orientation primarily governed how effectively the internal roads participated in carrying the tensile load. More favorable orientation–pattern combinations enabled a more stable stress transfer within the gauge section, whereas less favorable ones promoted earlier local damage through weaker bonded paths. This explained why pattern orientation showed the highest contribution to elastic modulus, tensile strength, and elongation [65, 66].

Additionally, to provide a comprehensive and quantitative comparison of the mechanical performance, the tensile test results of all specimens were detailed in Table 4. The average elastic modulus, tensile strength, and elongation values were presented together with their corresponding standard deviations.

3.2 Modal analysis for vibration response

FRF graphs of specimens were given in Fig. 6. Upon examining the graphs, a dominant resonance peak clearly representing the fundamental mode vibration behavior was identified in all specimens. This peak directly reflected the natural frequency of the specimens and their dynamic response under vibration.

Differences in peak position and curve shape observed among the specimens demonstrated that the manufacturing parameters interacted in a complex manner with vibration behavior, causing each specimen to develop a unique frequency response.

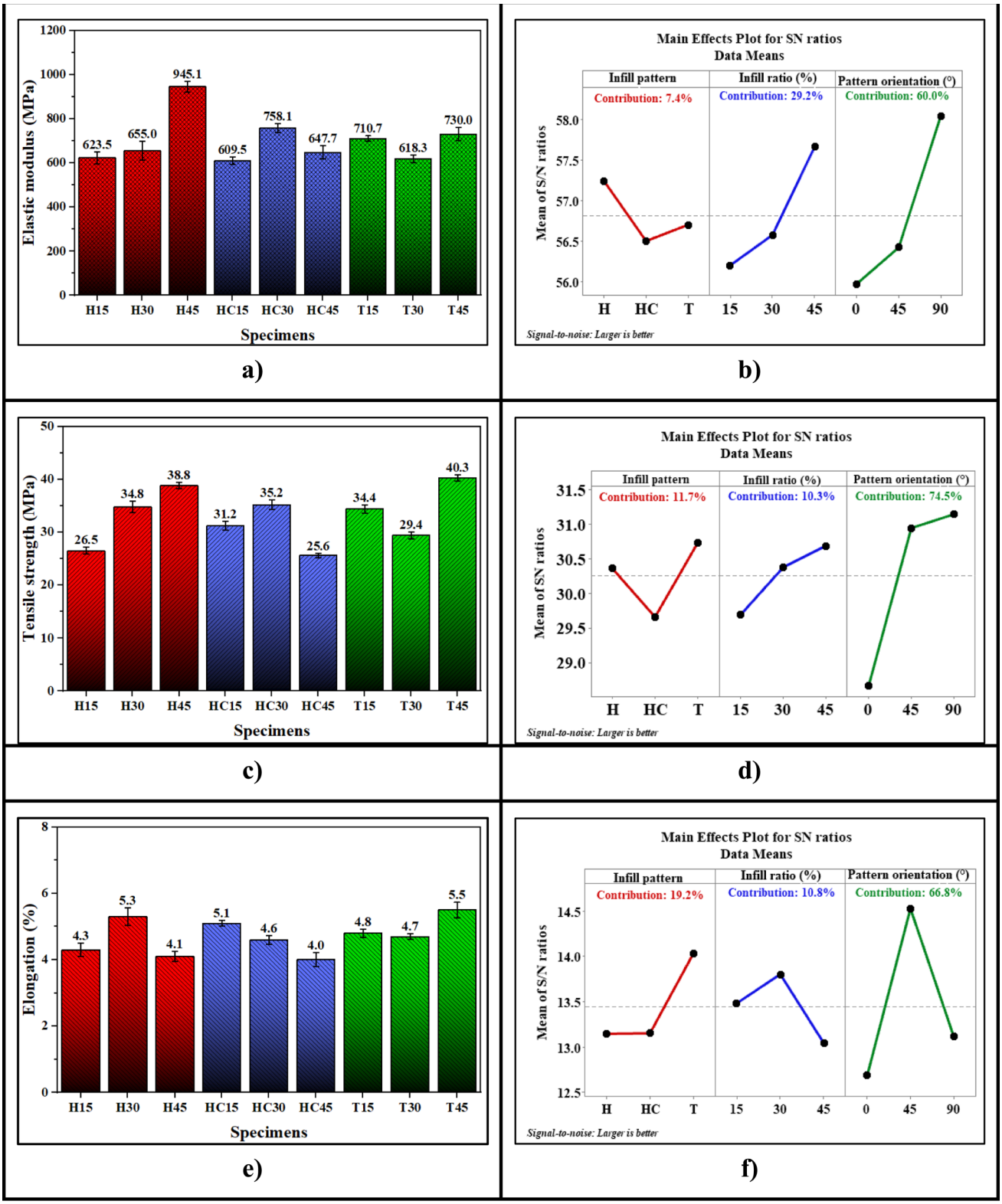


Fig. 5 Tensile test results of the specimens. **a** elastic modulus, **c** tensile strength, and **e** elongation, with corresponding S/N ratios shown in **b**, **d**, and **f**, respectively

Table 4 Tensile test results for all specimens

Specimen	Elastic modulus (MPa)	Tensile strength (MPa)	Elongation (%)
H15	623.5±26.8	26.5±0.6	4.3±0.2
H30	655.0±42.5	34.8±1.1	5.3±0.3
H45	945.1±24.9	38.8±0.6	4.1±0.2
HC15	609.5±18.1	31.2±0.9	5.1±0.1
HC30	758.1±19.3	35.2±1.0	4.6±0.1
HC45	647.7±29.6	25.6±0.4	4.0±0.2
T15	710.7±11.8	34.4±0.8	4.8±0.1
T30	618.3±18.2	29.4±0.6	4.7±0.1
T45	730.0±30.0	40.3±0.6	5.5±0.2

Figure 7 presented the modal test results of the specimens along with their corresponding S/N ratios. The stiffness values clearly demonstrated the effect of the infill pattern on the continuity of the load-bearing paths. The stiffness coefficient is directly proportional to the flexural rigidity EI for a prismatic beam with fixed geometry. The infill pattern and ratio used in this study varied. Therefore, the ranking of the infill configurations in terms of elastic modulus did not fully coincide with their stiffness coefficients. The highest stiffness values were obtained in the HC45 (450,000 N/m) and HC15 (213,000 N/m) specimens. The fractal-based "space-filling" structure of the Hilbert curve pattern contributed to increased deformation resistance in the elastic region by making the load transfer paths continuous and multidirectional. This behavior was consistent with the literature, which reported that complex curved geometries provide advantages, particularly in terms of stiffness [67]. Conversely, the lowest stiffness values were measured in the T15 (27,400 N/m) and T45 (23,600 N/m) specimens. In this case, the localization of load transfer due to the geometric structure led to a significant increase in stiffness loss in structures with less complex geometries, as similarly reported in previous studies [68, 69]. ANOVA analysis showed that the infill pattern was the most dominant parameter with a 59.1% contribution, confirming that stiffness was directly determined by the pattern geometry.

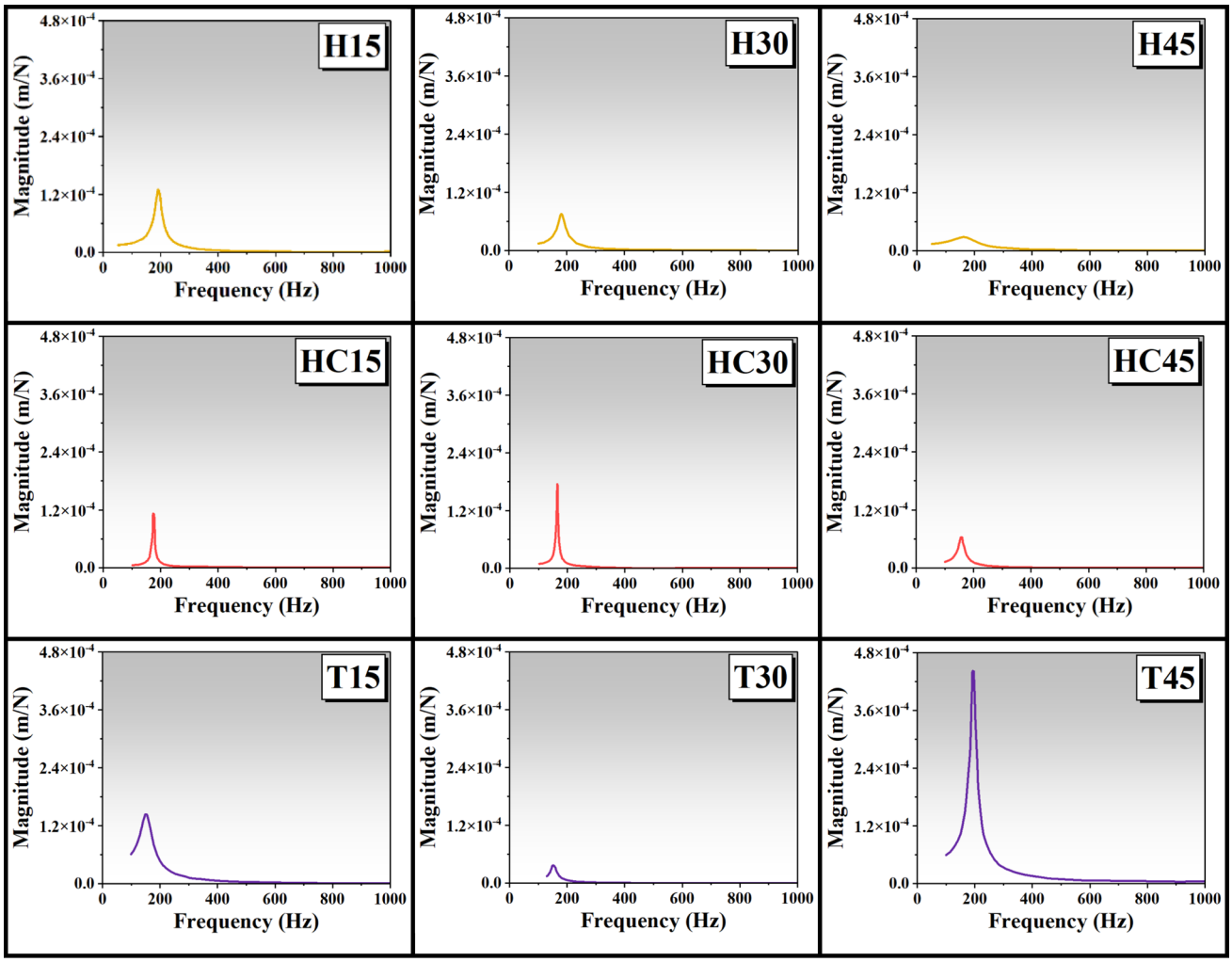


Fig. 6 FRF graphs of specimens

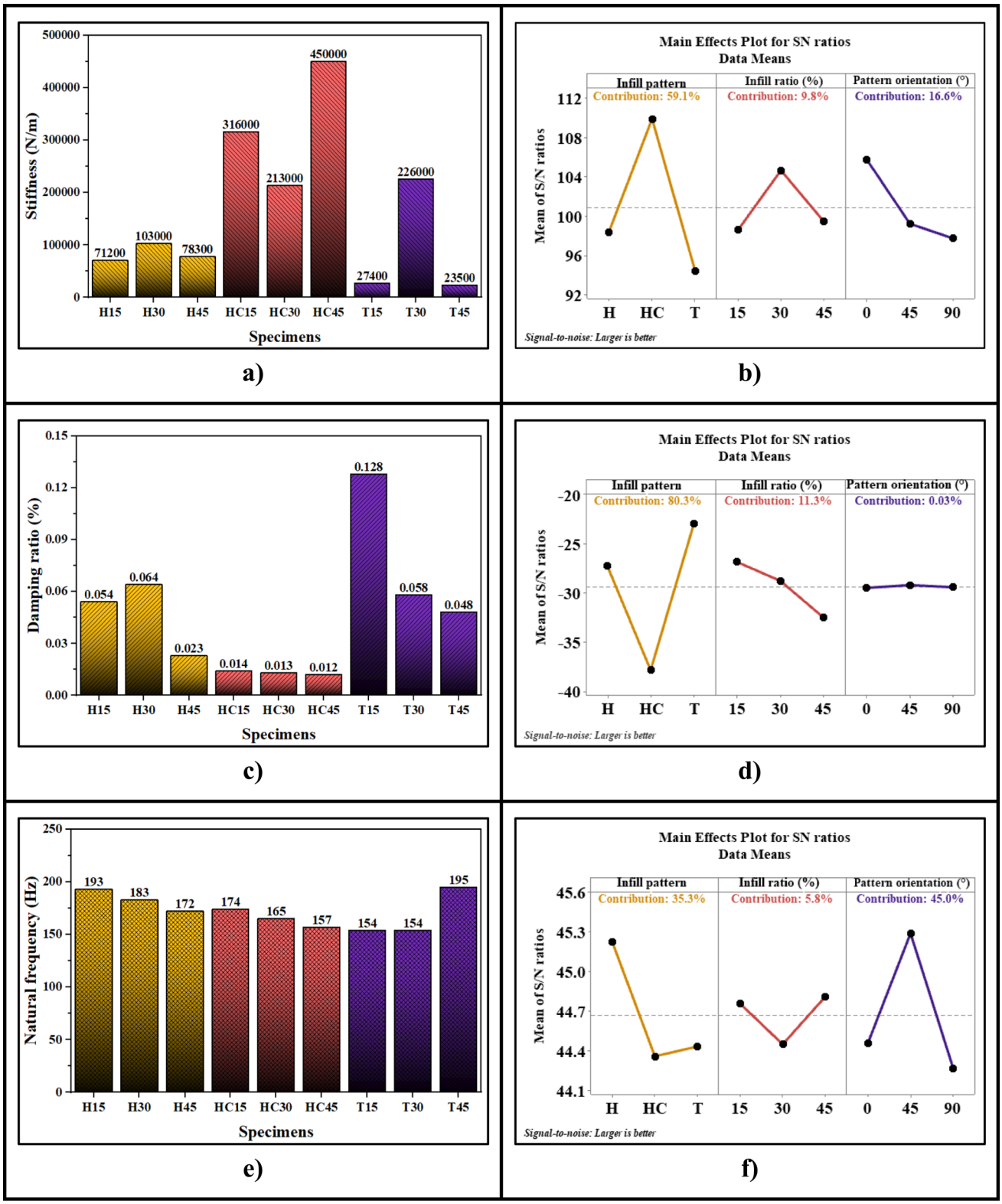


Fig. 7 Modal test results of the specimens. **a** stiffness, **c** damping ratio, and **e** natural frequency, with corresponding S/N ratios shown in **b**, **d**, and **f**, respectively

When the damping ratio results were examined, the highest value was detected for the T15 specimen (0.128%). This high damping ratio could be attributed to the micro-scale slip and energy absorption regions formed by the tetrahedral pattern. This behavior aligned with literature studies indicating that intersecting infill paths increase internal friction in polymer structures, thereby enhancing damping [43, 70, 71]. The lowest damping ratios were determined in the HC15 (0.014%), HC30 (0.013%), and HC45 (0.012%) specimens featuring the Hilbert curve pattern. ANOVA analysis showed that the infill pattern had the strongest effect on the damping ratio, contributing 80.3%, indicating that damping was influenced by internal topological friction, a mechanism distinct from elastic behavior. Additionally, the high infill ratio (45%) reduced internal voids, which enhanced inter-filament bonding and consequently increased internal friction. This provided a secondary contribution of 11.3% to the damping ratio of the specimens. Beyond the effect of topology alone, the damping response can also be interpreted in relation to the anisotropic deformation behavior of FFF-printed PLA [41, 56]. Since the printed roads and bonded interfaces do not deform identically in every direction under vibration, part of the input energy is dissipated through direction-dependent local slip, shear transfer, and friction between neighboring filaments [70, 71]. In this way, anisotropy influences not only how vibration is transmitted through the structure, but also how effectively it is attenuated, depending on the internal directional arrangement created by the selected infill design. This also helps explain why the Hilbert-based specimens exhibited high stiffness but very low damping, whereas the tetrahedral structure showed the highest damping response. In the Hilbert pattern, the continuity of the curved filament network increased resistance to deformation, while the same regular arrangement limited local interfacial motion and reduced frictional energy loss during vibration [72].

The highest natural frequency values were obtained in specimens T45 (195 Hz), H15 (193 Hz), and H30 (183 Hz). The highest frequency observed in the T45 specimen can specifically be explained by the tetrahedral network forming three-dimensional components and making the structure more resistant to mode shapes. These findings were compatible with studies reporting that regular lattice structures suppress resonance tendencies [59, 73]. Additionally, it is known that a structure's natural frequency is influenced by parameters such as elastic modulus, moment of inertia, and density. This leads to the natural frequency varying in a complex manner among specimens with different manufacturing parameters [1]. In this context, ANOVA analyses revealed that pattern orientation had the most significant effect on natural frequency with a contribution of 45.0%. Moreover, the infill pattern contributed substantially with 35.3%, indicating that natural frequency behavior was shaped by the interaction of anisotropic orientation and geometrical properties.

Table 5 Modal test results for all specimens

Specimen	Stiffness (N/m)	Damping ratio (%)	Natural frequency (Hz)
H15	71,200	0.054	193
H30	103,000	0.064	183
H45	78,300	0.023	172
HC15	316,000	0.014	174
HC30	213,000	0.013	165
HC45	450,000	0.012	157
T15	27,400	0.128	154
T30	226,000	0.058	154
T45	23,500	0.048	195

For the modal responses, the infill pattern exhibited the highest contribution to stiffness (59.1%) and damping ratio (80.3%), indicating that internal geometry was the dominant parameter affecting vibration behavior. Although strict statistical significance was not achieved for the modal responses, the lowest p-value in this group was obtained for the damping ratio ($p=0.095$), suggesting a tendency toward significance when considered together with the high contribution ratio. These findings indicated that internal geometry plays a decisive role in the vibration behavior of FFF-printed PLA specimens.

Additionally, the modal test results of all specimens were detailed in Table 5 to enable a comprehensive comparison. The stiffness, damping ratio, and natural frequency values were reported for each specimen.

4 Conclusions

This study demonstrated that the mechanical and vibration responses of FFF-printed PLA specimens can be effectively tailored through internal structural design. Within the investigated parameter range, pattern orientation primarily governed the tensile response, contributing 60.0% to elastic modulus, 74.5% to tensile strength, and 66.8% to elongation. The highest elastic modulus was obtained in specimen H45 (945.1 MPa), whereas the highest tensile strength and elongation were achieved by specimen T45, with values of 40.3 MPa and 5.5%, respectively. In contrast, infill pattern had the strongest influence on vibration-related responses, contributing 59.1% to stiffness and 80.3% to damping ratio. The highest stiffness was measured in specimen HC45 (450,000 N/m), the highest damping ratio was obtained in specimen T15 (0.128%), and the highest natural frequency was recorded in specimen T45 (195 Hz). These results

showed that different structural parameters do not control all performance metrics equally. In this context, it was detected that mechanical strength and dynamic behavior depend on different characteristics of the interior design.

From an engineering perspective, this finding is important because it shows that infill design can be used not only to reduce weight and material consumption but also to tune the functional behavior of printed components according to service requirements. For applications where tensile strength is critical, selecting a more favorable pattern orientation becomes decisive. In contrast, for components exposed to vibration, resonance, or oscillatory loading, the choice of infill topology is more important, since stiffness, damping capacity, and natural frequency can be adjusted through the internal geometry. This provides a practical design route for lightweight printed parts used in vibration-sensitive systems such as brackets, housings, fixtures, robotic components, and similar functional polymer structures. In this study, the results obtained provide a useful basis for FFF-printed structures. However, further investigations involving different materials, wider processing ranges, and more diverse service conditions are needed to support broader engineering generalization.

Future studies should therefore focus on broader experimental designs that can quantify factor interactions more explicitly, as well as on extending the analysis to different materials, environmental conditions, and loading scenarios. Numerical modeling approaches such as finite element analysis, together with fatigue and long-term vibration testing, would also be valuable for improving predictive capability and supporting the design of FFF-manufactured parts for real engineering applications.

Author contributions Gökhan Haydarlar: Investigation, Conceptualization, Writing – review & editing, Validation. Mehmet Alper Sofuoğlu: Writing—review & editing, Validation. Tevfik Oğuzhan Ergüder: Investigation, Conceptualization, Writing—review & editing, Validation. Semih Duran: Visualization, Investigation, Conceptualization, Writing—review & editing, Validation.

Funding Open access funding provided by the Scientific and Technological Research Council of Türkiye (TÜBİTAK).

Data availability Data will be made available on request.

Declarations

Conflict of interest The authors declare that they have no known competing financial interests or personal relationships that could have appeared to influence the work reported in this paper.

Open Access This article is licensed under a Creative Commons Attribution 4.0 International License, which permits use, sharing, adaptation, distribution and reproduction in any medium or format, as long as you give appropriate credit to the original author(s) and the source, provide a link to the Creative Commons licence, and indicate if changes were made. The images or other third party material in this article are included in the article's Creative Commons licence, unless indicated otherwise in a credit line to the material. If material is not included in the article's Creative Commons licence and your intended use is not permitted by statutory regulation or exceeds the permitted use, you will need to obtain permission directly from the copyright holder. To view a copy of this licence, visit http://creativecommons.org/licenses/by/4.0/.

References

1. Öteyaka MÖ, Çakir FH, Sofuoğlu MA (2022) Effect of infill pattern and ratio on the flexural and vibration damping characteristics of FDM printed PLA specimens. Mater Today Commun. https://doi.org/10.1016/j.mtcomm.2022.104912
2. Li X, Luo L, Wang L, Vusug B (2025) Bending strength measurement of structures printed via fused deposition modeling with different infill patterns. Sci Rep. https://doi.org/10.1038/s41598-025-24148-8
3. Frazier WE (2014) Metal additive manufacturing: a review. J Mater Eng Perform 23:1917–1928
4. Van Sice C, Faludi J (2021) Comparing environmental impacts of metal additive manufacturing to conventional manufacturing. Proceedings of the Design Society 1:671–680
5. Kozior T, Mamun A, Trabelsi M, et al (2020) Quality of the surface texture and mechanical properties of FDM printed samples after thermal and chemical treatment. J Mech Eng/Strojniški Vestnik 66
6. Modir A, Tansel I (2022) Analysis of force sensing accuracy by using SHM methods on conventionally manufactured and additively manufactured small polymer parts. Polymers 14:3755
7. Javaid M, Haleem A, Singh RP et al (2021) Role of additive manufacturing applications towards environmental sustainability. Adv Ind Eng Polymer Res 4:312–322
8. Joshi SC, Sheikh AA (2015) 3D printing in aerospace and its long-term sustainability. Virtual Phys Prototyping 10:175–185
9. Aimar A, Palermo A, Innocenti B (2019) The role of 3D printing in medical applications: a state of the art. J Healthc Eng 2019:5340616
10. Gao H, Zhang W, Yu Z et al (2021) Emerging applications of 3D printing in biomanufacturing. Trends Biotechnol 39:1114–1116
11. Nichols MR (2019) How does the automotive industry benefit from 3D metal printing? Met Powder Rep 74:257–258
12. Mulford JS, Babazadeh S, Mackay N (2016) Three-dimensional printing in orthopaedic surgery: review of current and future applications. ANZ J Surg 86:648–653
13. Pallottino F, Hakola L, Costa C et al (2016) Printing on food or food printing: a review. Food Bioproc Tech 9:725–733
14. Nasution A, Hakim ML, Herianto H, Rifai AP (2026) Flexural performance and interfacial bonding of PLA/ABS/HIPS composites in multi-nozzle 3D printing. J Brazilian Soc Mech Sci Eng. https://doi.org/10.1007/s40430-025-06033-7
15. Çakır FH, Er Ü, Tekkalmaz M, Sofuoğlu MA (2025) Evaluation of electromechanical impedance, modal and X-ray testing as non-destructive methods for additively manufactured plastics. Nondestruct Testing Eval. https://doi.org/10.1080/10589759.2025.2500552
16. Standard A (2012) Standard terminology for additive manufacturing technologies. ASTM International F2792–12a 46:10918–10928
17. Ramírez IS, Márquez FPG, Papaelias M (2023) Review on additive manufacturing and non-destructive testing. J Manuf Syst 66:260–286

18. Xue F, Robin G, Boudaoud H, et al Effect of process parameters on the vibration properties of PLA structure fabricated by additive manufacturing
19. Gumpinger J, Seifi M, Shamsaei N, et al (2021) Recent progress on global standardization. Fundamentals of laser powder bed fusion of metals 563–582
20. Gao X, Yu N, Li J (2020) Influence of printing parameters and filament quality on structure and properties of polymer composite components used in the fields of automotive. In: Structure and properties of additive manufactured polymer components. Elsevier, pp 303–330
21. Pramanik D, Roy N, Kuar AS (2022) Additive manufacturing of polymer materials: recent developments
22. Shanmugam V, Das O, Babu K et al (2021) Fatigue behaviour of FDM-3D printed polymers, polymeric composites and architected cellular materials. Int J Fatigue 143:106007
23. Pathek IA, da Silva JRF, Lima DD et al (2024) Assessment of carbon fiber incorporation effects on overall characteristics and properties of 3D-printed PLA. J Brazilian Soc Mech Sci Eng. https://doi.org/10.1007/s40430-024-05233-x
24. Gupta A, Meshram JR, Singh M et al (2025) Experimental and numerical studies on the contributions of the different geometric and process parameters on 3D printed PLA pin joints. J Brazilian Soc Mech Sci Eng. https://doi.org/10.1007/s40430-025-05690-y
25. Öteyaka MÖ, Aybar K, Öteyaka HC (2021) Effect of infill ratio on the tensile and flexural properties of unreinforced and carbon fiber-reinforced polylactic acid manufactured by fused deposition modeling. J Mater Eng Perform 30:5203–5215
26. Penumakala PK, Santo J, Thomas A (2020) A critical review on the fused deposition modeling of thermoplastic polymer composites. Compos B Eng 201:108336
27. Wickramasinghe S, Do T, Tran P (2020) FDM-based 3D printing of polymer and associated composite: a review on mechanical properties, defects and treatments. Polymers (Basel) 12:1529
28. Buchanan C, Gardner L (2019) Metal 3D printing in construction: a review of methods, research, applications, opportunities and challenges. Eng Struct 180:332–348
29. Wittbrodt B, Pearce JM (2015) The effects of PLA color on material properties of 3-D printed components. Addit Manuf 8:110–116
30. Chacón JM, Caminero MA, García-Plaza E, Núnez PJ (2017) Additive manufacturing of PLA structures using fused deposition modelling: effect of process parameters on mechanical properties and their optimal selection. Mater Des 124:143–157
31. Liu Z, Lei Q, Xing S (2019) Mechanical characteristics of wood, ceramic, metal and carbon fiber-based PLA composites fabricated by FDM. J Mater Res Technol 8:3741–3751
32. Çelebi A (2019) Investigation of fused deposition modeling processing parameters of 3D PLA specimens by an experimental design methodology. Materials Testing 61:405–410
33. Carrasco F, Pagès P, Gámez-Pérez J et al (2010) Processing of poly (lactic acid): characterization of chemical structure, thermal stability and mechanical properties. Polym Degrad Stab 95:116–125
34. Passari ÉS, Lauermann CH, Bortoli TJ et al (2026) Mechanical performance optimization of pla-graphene composites using the Taguchi method. J Brazilian Soc Mech Sci Eng. https://doi.org/10.1007/s40430-025-06079-7
35. Akhoundi B, Behravesh AH (2019) Effect of filling pattern on the tensile and flexural mechanical properties of FDM 3D printed products. Exp Mech 59:883–897. https://doi.org/10.1007/s11340-018-00467-y
36. Sun Q, Rizvi GM, Bellehumeur CT, Gu P (2008) Effect of processing conditions on the bonding quality of FDM polymer filaments. Rapid Prototyp J 14:72–80
37. Mwema FM, Akinlabi ET (2020) Basics of fused deposition modelling (FDM). In: Fused deposition modeling: strategies for quality enhancement. Springer, pp 1–15
38. León-Calero M, Reyburn Valés SC, Marcos-Fernández Á, Rodríguez-Hernandez J (2021) 3D printing of thermoplastic elastomers: role of the chemical composition and printing parameters in the production of parts with controlled energy absorption and damping capacity. Polymers (Basel) 13:3551
39. Medel F, Abad J, Esteban V (2022) Stiffness and damping behavior of 3D printed specimens. Polym Test 109:107529
40. Dobos J, Hanon MM, Oldal I (2022) Effect of infill density and pattern on the specific load capacity of FDM 3D-printed PLA multi-layer sandwich. J Polym Eng 42:118–128. https://doi.org/10.1515/polyeng-2021-0223
41. Ahn SH, Baek C, Lee S, Ahn IS (2003) Anisotropic tensile failure model of rapid prototyping parts-fused deposition modeling (FDM). Int J Mod Phys B 17:1510–1516
42. Bellehumeur C, Li L, Sun Q, Gu P (2004) Modeling of bond formation between polymer filaments in the fused deposition modeling process. J Manuf Process 6:170–178
43. He F, Ning H, Khan M (2023) Effect of 3D printing process parameters on damping characteristic of cantilever beams fabricated using material extrusion. Polymers (Basel) 15:257
44. Mohan E, Saravana Kumar M (2022) Experimental investigation on mechanical and tribological properties of the fused filament fabrication of poly-lactic acid parts with various print orientations. Appl Phys A Mater Sci Process. https://doi.org/10.1007/s00339-022-05579-w
45. Buss C, Reci F, Hribernig T, Steininger S (2026) Experimental investigation into the influence of infill density, print pattern, and built-up direction on the flexural strength of FFF-manufactured PLA components. J Manuf Mater Proc 10:21
46. Singh J, Goyal KK, Kumar R (2022) Effect of filling percentage and raster style on tensile behavior of FDM produced PLA parts at different build orientation. Mater Today Proc 63:433–439
47. Hikmat M, Rostam S, Ahmed YM (2021) Investigation of tensile property-based Taguchi method of PLA parts fabricated by FDM 3D printing technology. Results Eng 11:100264
48. Bonada J, Pastor MM, Buj-Corral I (2021) Influence of infill pattern on the elastic mechanical properties of fused filament fabrication (FFF) parts through experimental tests and numerical analyses. Materials 14:5459
49. Gonabadi H, Chen Y, Yadav A, Bull S (2022) Investigation of the effect of raster angle, build orientation, and infill density on the elastic response of 3D printed parts using finite element microstructural modeling and homogenization techniques. Int J Adv Manuf Technol 118:1485–1510
50. Park J-H, Kim KJ (2013) Optimal design of camber link component for light weight automobile using CAE (computer aided engineering). Int J Precis Eng Manuf 14:1433–1437
51. Gibson RF (2010) A review of recent research on mechanics of multifunctional composite materials and structures. Compos Struct 92:2793–2810
52. Madeira JFA, Araújo AL, Soares CMM et al (2015) Multiobjective design of viscoelastic laminated composite sandwich panels. Compos B Eng 77:391–401
53. Johnson CD, Kienholz DA (1982) Finite element prediction of damping in structures with constrained viscoelastic layers. AIAA J 20:1284–1290
54. Li Z, Crocker MJ (2006) Effects of thickness and delamination on the damping in honeycomb–foam sandwich beams. J Sound Vib 294:473–485
55. Sofuoğlu MA, Çakır FH, Çelikten S (2021) Influence of steel fiber addition on the vibrational characteristic of high strength cementitious composites. Arab J Sci Eng 46:4677–4685

56. He F, Khan M (2021) Effects of printing parameters on the fatigue behaviour of 3D-printed ABS under dynamic thermo-mechanical loads. Polymers (Basel) 13:2362
57. de Oliveira TL, de Carvalho J (2021) Design and numerical evaluation of quadrotor drone frame suitable for fabrication using fused filament fabrication with consumer-grade ABS. J Braz Soc Mech Sci Eng 43:436. https://doi.org/10.1007/s40430-021-03160-9
58. Chaitanya SK, Reddy KM, Harsha S (2015) Vibration properties of 3D printed/rapid prototype parts. Int J Innov Res Sci Eng Technol 4:4602–4608
59. Marshall J, Allen RA, McGray CD, Geist J (2010) MEMS Young's modulus and step height measurements with round robin results. J Res Natl Inst Stand Technol 115:303
60. Putro AJN, Purnomo E, Yuda Purnomo DJ et al (2025) Optimizing performance of hybrid PLA-GFRP composites by using honeycomb pattern and VARI reinforcement. Mater Lett. https://doi.org/10.1016/j.matlet.2025.138618
61. Ivorra-Martinez J, Quiles-Carrillo L, Lascano D et al (2020) Effect of infill parameters on mechanical properties in additive manufacturing. Dyna (Spain) 95:412–417. https://doi.org/10.6036/9674
62. Tymrak BM, Kreiger M, Pearce JM (2014) Mechanical properties of components fabricated with open-source 3-D printers under realistic environmental conditions. Mater Des 58:242–246. https://doi.org/10.1016/j.matdes.2014.02.038
63. Qamar Tanveer M, Mishra G, Mishra S, Sharma R (2022) Effect of infill pattern and infill density on mechanical behaviour of FDM 3D printed Parts—a current review. Mater Today Proc 62:100–108. https://doi.org/10.1016/j.matpr.2022.02.310
64. Doshi M, Mahale A, Singh SK, Deshmukh S (2021) Printing parameters and materials affecting mechanical properties of FDM-3D printed Parts: Perspective and prospects. In: Materials Today: Proceedings. Elsevier Ltd, pp 2269–2275
65. Kannan S, Vezhavendhan R, Kishore S, Kanumuru KV (2020) Investigating the effect of orientation, infill density with Triple raster pattern on the tensile properties for 3D Printed samples. IOP SciNotes 1:024405. https://doi.org/10.1088/2633-1357/abb290
66. Ayatollahi MR, Nabavi-Kivi A, Bahrami B et al (2020) The influence of in-plane raster angle on tensile and fracture strengths of 3D-printed PLA specimens. Eng Fract Mech. https://doi.org/10.1016/j.engfracmech.2020.107225
67. Zhang Z, Scarpa F, Bednarcyk BA, Chen Y (2021) Harnessing fractal cuts to design robust lattice metamaterials for energy dissipation. Addit Manuf. https://doi.org/10.1016/j.addma.2021.102126
68. Schwahofer O, Büttner S, Colin D, Drechsler K (2023) Tailored elastic properties of beam-based lattice unit structures. Int J Mech Mater Des 19:927–949. https://doi.org/10.1007/s10999-023-09659-4
69. Wang X, Xu S, Zhou S et al (2016) Topological design and additive manufacturing of porous metals for bone scaffolds and orthopaedic implants: a review. Biomaterials 83:127–141
70. Tang X, Yan X (2020) A review on the damping properties of fiber reinforced polymer composites. J Ind Text 49:693–721
71. Rao SS (2019) Vibration of continuous systems. John Wiley & Sons
72. Xu X, Song H, Wang L (2023) Cushioning performance of hilbert fractal sandwich packaging structures under quasi-static compressions. Comput Model Eng Sci 135:275–292. https://doi.org/10.32604/cmes.2022.022637
73. Andresen S, Bäger A, Hamm C (2020) Eigenfrequency maximisation by using irregular lattice structures. J Sound Vib. https://doi.org/10.1016/j.jsv.2019.115027

Publisher's Note Springer Nature remains neutral with regard to jurisdictional claims in published maps and institutional affiliations.